

ORIGINAL ARTICLE

Nondiagnostic, radial-probe endobronchial ultrasound-guided biopsy for peripheral lung lesions: The added value of radiomics from ultrasound imaging for predicting malignancy

Jihwan Choi^{1,2} | Sungmin Zo³ | Jong Hoon Kim⁴ | You Jin Oh⁵  |
Joong Hyun Ahn⁶ | Myoungkyoung Kim⁷ | Kyungjong Lee³ | Ho Yun Lee^{5,7} 

¹Department of Digital Health, SAIHST, Sungkyunkwan University, Seoul, South Korea

²Hongseong-gun Public Health Center, Hongseong-gun, South Korea

³Division of Pulmonary and Critical Care Medicine, Department of Medicine, Samsung Medical Center, Sungkyunkwan University School of Medicine, Seoul, South Korea

⁴Industrial Biomaterial Research Center, Korea Research Institute of Bioscience and Biotechnology, Daejeon, South Korea

⁵Department of Health Sciences and Technology, SAIHST, Sungkyunkwan University, Seoul, South Korea

⁶Biomedical Statistics Center, Data Science Research Institute, Research Institute for Future Medicine, Samsung Medical Center

⁷Department of Radiology and Center for Imaging Science, Samsung Medical Center, Sungkyunkwan University School of Medicine, Seoul, South Korea

Correspondence

Ho Yun Lee, Department of Radiology and Center for Imaging Science, Samsung Medical Center, Sungkyunkwan University School of Medicine, 81 Irwon-Ro, Gangnam-Gu, Seoul 06351, South Korea.
Email: hoyunlee96@gmail.com

Kyungjong Lee, Division of Pulmonary and Critical Care Medicine, Department of Medicine, Samsung Medical Center, Sungkyunkwan University School of Medicine, 81 Irwon-Ro, Gangnam-Gu, Seoul 06351, South Korea.
Email: kj2011.lee@gmail.com

Funding information

Future Medicine 20*30 Project of the Samsung Medical Center, Grant/Award Number: #SMO1220071; National Research Foundation of Korea (NRF) grant funded by the Korean government (MSIT), Grant/Award Number: NRF-2022R1A2C1003999

Abstract

Objectives: This study investigated whether radiomic features extracted from radial-probe endobronchial ultrasound (radial EBUS) images can assist in decision-making for subsequent clinical management in cases with indeterminate pathologic results.

Methods: A total of 494 patients who underwent radial EBUS biopsy for lung nodules between January 2017 and December 2018 were allocated to our training set. For the validation set, 229 patients with radial EBUS biopsy results from January 2019 to April 2020 were used. A multivariate logistic regression analysis was used for feature selection and prediction modeling.

Results: In the training set, 157 (67 benign and 90 malignant) of 212 patients pathologically diagnosed as indeterminate were analyzed. In the validation set, 213 patients were diagnosed as indeterminate, and 158 patients (63 benign and 95 malignant) were included in the analysis. The performance of the radiomics-added model, which considered satellite nodules, linear arc, shape, patency of vessels and bronchi, echogenicity, spiculation, C-reactive protein, and minimum histogram, was 0.929 for the training set and 0.877 for the validation set, whereas the performance of the model without radiomics was 0.910 and 0.891, respectively.

Conclusion: Although the next diagnostic step for indeterminate lung biopsy results remains controversial, integrating various factors, including radiomic features from radial EBUS, might facilitate decision-making for subsequent clinical management.

KEYWORDS

bronchoscopy, diagnostic imaging, lung neoplasm, pathology, ultrasound

Jihwan Choi and Sungmin Zo contributed equally as co-first authors.

This is an open access article under the terms of the [Creative Commons Attribution-NonCommercial-NoDerivs](https://creativecommons.org/licenses/by-nc-nd/4.0/) License, which permits use and distribution in any medium, provided the original work is properly cited, the use is non-commercial and no modifications or adaptations are made.

© 2022 The Authors. *Thoracic Cancer* published by China Lung Oncology Group and John Wiley & Sons Australia, Ltd.

INTRODUCTION

Radial-probe endobronchial ultrasound (EBUS) has been reported to be useful in identifying and taking samples of peripheral pulmonary lesions, improving the diagnostic sensitivity of advanced bronchoscopic techniques.^{1,2} However, when biopsy results are indeterminate, the next diagnostic step for pathologically indeterminate cases remains uncertain.³

Several attempts have been made to improve the diagnostic yield of radial EBUS, but they were mostly classical models for calculating the probability of malignancy based on clinical factors such as age, sex, smoking history, and

malignancy history and semantic radiological features on chest computed tomography (CT) images.^{3,4} Recent studies have shown that those models could be reinforced with additional features from radial EBUS.^{5,6} Nevertheless, higher prediction performance is required for those models to be applicable in clinical settings, and variables that describe tumors in more detail are needed to construct a better prediction model.

Radiomics is a rapidly evolving technology for extracting quantitative information from extensive medical images and has attracted considerable interest in the field of radiology.⁷⁻¹⁰ Its application is most promising in oncology, and numerous studies have incorporated radiomics

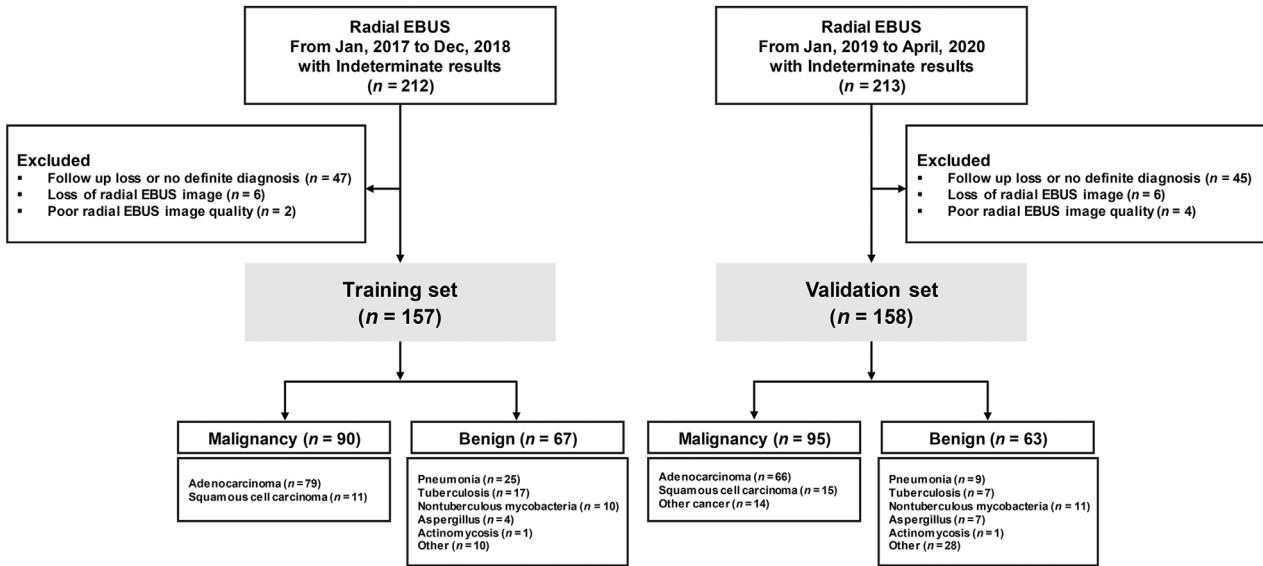


FIGURE 1 Initial radial EBUS results and final diagnoses for the training and validation sets. Other includes cryptococcosis, sarcoidosis, *Toxocara canis*, and mucocele. Radial EBUS, radial probe endobronchial ultrasound.

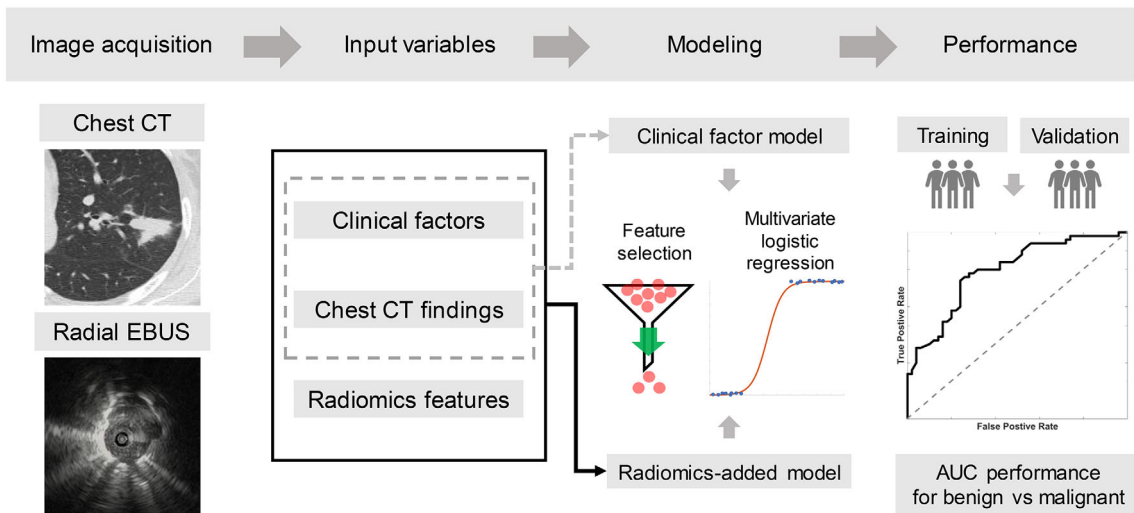


FIGURE 2 Method flowchart. The clinical factor model was built using demographic and clinical factors and CT and semantic ultrasound features. Radiomic features from radial EBUS were additionally considered in the radiomics-based model. The relationships among the variables were analyzed and models were constructed. For the training and validation sets, the AUC performance of each model was calculated. AUC, area under the curve.

for diagnostic, prognostic, and predictive purposes.^{11–13} Those approaches provide a deeper understanding of tumor biology and behavior and therefore, improve the performance of prediction models. In this work, we developed and validated a radiomics-added malignancy prediction model with two independent cohorts to further classify patients whose lesions were initially diagnosed as indeterminate. We have demonstrated its predictive performance and potential to facilitate decision-making about subsequent clinical management of patients with indeterminate pathologic results.

MATERIALS AND METHODS

Patients

This study was approved by the Institutional Review Board of Samsung Medical Center, and informed consent was waived (IRB No. 2018-03-021) because it was retrospective. We reviewed the medical records of 494 patients and 229 patients, all of whom underwent radial EBUS biopsy for lung nodules at Samsung Medical Center between January 2017 and December 2018 and between January

TABLE 1 Baseline characteristics of patients in the training and validation sets

| Characteristics | Training set (<i>n</i> = 157) | Validation set (<i>n</i> = 158) | <i>p</i> -value |
|-----------------------------|--------------------------------|----------------------------------|-----------------|
| Final diagnosis | | | 0.696 |
| Benign | 67 (42.7) | 63 (59.9) | |
| Malignant | 90 (57.3) | 95 (60.1) | |
| Clinical factors | | | |
| Age, y | 66.0 (59.0–73.0) | 66.0 (59.0–72.0) | 0.877 |
| Sex | | | 0.535 |
| Male | 91 (58.0) | 98 (62.0) | |
| Female | 66 (42.0) | 60 (38.0) | |
| Smoking history (yes) | 69 (43.9) | 86 (54.4) | 0.081 |
| History of malignancy (yes) | 30 (19.1) | 21 (13.3) | 0.212 |
| Chest CT findings | | | |
| Size, mm | 27.0 (19.0, 37.0) | 26.0 (19.0, 34.0) | 0.721 |
| Upper lobe | 84 (53.5) | 77 (48.7) | 0.463 |
| Type | | | 0.189 |
| Solid | 110 (70.1) | 122 (77.2) | |
| Part-solid | 47 (29.9) | 36 (22.8) | |
| Spiculation | 56 (35.7) | 43 (27.2) | 0.135 |
| Bronchus sign | 48 (30.6) | 57 (36.1) | 0.359 |
| Satellite nodules | 44 (28.0) | 44 (27.8) | 1.000 |
| Radial EBUS findings | | | |
| Echogenicity | | | 0.962 |
| Homogeneous | 83 (57.3) | 92 (58.2) | |
| Heterogeneous | 67 (42.7) | 66 (41.8) | |
| Attenuation | 59 (37.6) | 72 (45.6) | 0.185 |
| Margin | | | 0.001 |
| Regular | 22 (14.0) | 47 (29.7) | |
| Irregular | 135 (86.0) | 111 (70.3) | |
| Shape | | | 0.609 |
| Round/oval | 71 (45.2) | 77 (48.1) | |
| Complex | 86 (54.8) | 81 (51.3) | |
| Dots | 43 (27.4) | 37 (23.4) | 0.496 |
| Linear arc | 56 (35.7) | 64 (40.5) | 0.443 |
| Vessels and bronchi | | | 0.047 |
| Patent | 28 (17.8) | 44 (28.7) | |
| Not patent | 129 (82.2) | 114 (72.2) | |

Note: Unless otherwise indicated, data are numbers of patients with percentages in parentheses. Data are median; data in parentheses are the interquartile range. Abbreviations: CT, computed tomography; radial EBUS, radial probe endobronchial ultrasound.

2019 and April 2020, respectively. Each patient group was prepared independently, and they were used as the training and validation sets (Figure 1). Demographic and clinical data, such as age, sex, smoking history, malignancy history, peripheral blood lab data, and final diagnosis, were retrieved from the medical records. Patients were excluded if (1) they were lost to follow up or had no definite diagnosis; (2) radial EBUS images were missing from the record; or (3) radial EBUS image quality was inadequate for analysis.

All patients undergoing radial EBUS were classified as “positive for malignancy” or “indeterminate,” based on the biopsy obtained using radial EBUS. “Positive for

malignancy” indicates a primary or metastatic cancer found in a radial EBUS-guided biopsy. “Indeterminate” results included atypical cells, granuloma, fibrosis, and inflammation and did not exclude the possibility of malignancy. Among those, only patients diagnosed pathologically as indeterminate through radial EBUS biopsy were included in this study.

Definitive diagnoses were defined as those (1) pathologically confirmed as cancerous by endobronchial ultrasound-guided transbronchial needle aspiration, surgical specimen analysis, a core needle biopsy, or additional radial EBUS, or (2) with culture results from sputum or bronchial washing that showed tuberculosis or atypical mycobacteria with appropriate

TABLE 2 Baseline characteristics of patients in the training and validation sets by malignancy status

| Characteristics | Training set | | P-value | Validation set | | p-value |
|-----------------------------|-----------------|--------------------|---------|-------------------|--------------------|---------|
| | Benign (n = 67) | Malignant (n = 90) | | Benign (n = 63) | Malignant (n = 95) | |
| Clinical factors | | | | | | |
| Age, y | 66 (58.0, 72.5) | 66.5 (59.0, 73.0) | 0.756 | 65.0 (58.0, 70.0) | 68 (59.0, 73.0) | 0.045 |
| Sex | | | 0.384 | | | 0.069 |
| Male | 42 (62.7) | 49 (54.4) | | 45 (71.4) | 53 (55.8) | |
| Female | 25 (37.3) | 41 (45.6) | | 18 (28.6) | 42 (44.2) | |
| Smoking history (yes) | 29 (43.3) | 40 (44.4) | 1.000 | 32 (50.8) | 54 (56.8) | 0.559 |
| History of malignancy (yes) | 10 (14.9) | 20 (22.2) | 0.345 | 6 (9.5) | 15 (15.8) | 0.370 |
| Chest CT findings | | | | | | |
| Size, mm | 27 (19.0, 37.5) | 27 (20.0, 35.8) | 0.960 | 25 (19.0, 41.0) | 26 (19.5, 33.0) | 0.710 |
| Upper lobe | 28 (41.8) | 56 (62.2) | 0.017 | 29 (46.0) | 48 (50.5) | 0.696 |
| Type | | | 0.108 | | | 0.955 |
| Solid | 15 (22.4) | 32 (35.6) | | 15 (23.8) | 21 (22.1) | |
| Part-solid | 52 (77.6) | 58 (64.4) | | 48 (76.2) | 74 (77.9) | |
| Spiculation | 11 (16.4) | 45 (50.0) | <0.001 | 13 (20.6) | 30 (31.6) | 0.183 |
| Bronchus sign | 12 (17.9) | 36 (40.0) | <0.005 | 19 (30.2) | 38 (40.0) | 0.275 |
| Satellite nodule | 34 (50.7) | 10 (11.1) | <0.001 | 32 (50.8) | 12 (12.6) | <0.001 |
| Radial EBUS findings | | | | | | |
| Echogenicity | | | <0.001 | | | <0.001 |
| Homogeneous | 52 (77.6) | 38 (42.2) | | 53 (84.1) | 39 (41.1) | |
| Heterogeneous | 15 (22.4) | 52 (57.8) | | 10 (15.9) | 56 (58.9) | |
| Attenuation | 18 (26.9) | 41 (45.6) | 0.026 | 17 (27.0) | 55 (57.9) | <0.001 |
| Margin | | | 0.017 | | | 0.181 |
| Regular | 15 (22.4) | 7 (7.8) | | 23 (36.5) | 50 (25.3) | |
| Irregular | 52 (77.6) | 83 (92.2) | | 40 (63.5) | 71 (74.7) | |
| Shape | | | 0.817 | | | 0.948 |
| Round/oval | 13 (19.4) | 20 (22.2) | | 30 (47.6) | 47 (48.4) | |
| Complex | 54 (80.6) | 70 (77.8) | | 33 (52.4) | 48 (50.5) | |
| Dots | 8 (11.9) | 35 (38.9) | <0.001 | 8 (12.7) | 29 (30.5) | 0.016 |
| Linear arc | 9 (13.4) | 47 (52.2) | <0.001 | 20 (31.7) | 44 (46.3) | 0.097 |
| Vessels and bronchi | | | <0.001 | | | <0.001 |
| Patent | 23 (34.3) | 5 (5.6) | | 36 (57.1) | 8 (8.4) | |
| Not patent | 44 (65.7) | 85 (94.4) | | 27 (42.9) | 87 (91.6) | |

Note: Unless otherwise indicated, data are numbers of patients with percentages in parentheses. Data are median; data in parentheses are the interquartile range. Abbreviations: CT, computed tomography; radial EBUS, radial probe endobronchial ultrasound.

antibiotic response, or (3) with follow-up chest CT implying resolved or improved lesions and a reassessment by a radiologist that confirmed the possibility of benignity. In these cases, the patients were observed for at least 6 months.¹⁴

The CT images were obtained before the radial EBUS biopsy with the following parameters: detector collimation, 1.25 or 0.625 mm, scans performed at 120 kVp with 150–200 mA, and a reconstruction interval of 1–2.5 mm.¹⁵

Procedure

To evaluate the tracheobronchial tree, bronchoscopic evaluation was performed under conscious sedation induced with midazolam and fentanyl before radial EBUS-guided biopsy. A 4-mm bronchoscope (BF P260F; Olympus) was used to approach the sub-subsegmental level closest to the suspected tumor area after reviewing chest CT or positron emission tomography-CT images. Then radial EBUS probe (1.4-mm, 20-MHz, UM S20-17 S; Olympus) was inserted through the bronchoscope working channel. When the target mass lesion was found on ultrasonography, the length of the probe inserted from the tip of the radial EBUS to the outer level of the working channel was measured. After removing the probe, a 1.8-mm biopsy forceps was marked at the same length using tape and inserted through the working channel for transbronchial lung biopsy. Although no additional guide sheath or fluoroscopy was used, radial EBUS probe was administered alternately with biopsy

forceps multiple times, to recheck the lesion that is being biopsied.¹⁶

Imaging and interpretation

Ultrasound images showing the tumors targeted during the radial EBUS procedure were digitally captured. A region of interest (ROI) was automatically drawn on all captured ultrasound images using commercial software (Aview, version 1.0.23, 2018; Coreline Soft) to construct a volume of interest that included the whole target lesion.¹⁷ A pulmonologist made additional manual corrections to each ROI.

From the ROIs, 34 quantitative ultrasound radiomic features characterizing the tumor margin were extracted. The features were classified into three categories: (1) histogram features after applying Laplace of Gaussian (LoG) filters; (2) gray level co-occurrence matrix (GLCM) features; and (3) gray level size zone matrix (GLSZM) features. The histogram features represent the range and frequency of the tumor pixel values within the defined lesion ROI. The LoG requires the use of a Gaussian smoothing filter to reduce noise in the CT and then a Laplacian filter is applied to highlight regions of rapid intensity change. As the texture-based feature, two feature sets, GLCM and GLSZL were used as follows: GLCM describes the second-order joint probability function of an image region and considers the association between neighboring voxels, and GLSZM quantifies gray level zones, defined as the number of connected voxels that

TABLE 3 Comparison of predictive performance between the clinical factor model and radiomics-added model

| Prediction models | Selected variables in model | Univariate analysis OR (95% CI) | Multivariate analysis OR (95% CI) | Performance in training set (AUC) | Performance in validation set (AUC) |
|------------------------------------|----------------------------------|---------------------------------|-----------------------------------|-----------------------------------|-------------------------------------|
| Clinical factor model ^a | Spiculation | 5.09 (2.43, 11.40) | 3.57 (1.32, 10.42) | 0.910 | 0.891 |
| | Satellite nodule | 0.12 (0.05, 0.27) | 0.05 (0.01, 0.14) | | |
| | Upper lobe | 2.29 (1.21, 4.41) | 3.17 (1.25, 8.54) | | |
| | Echogenicity | 4.74 (2.37, 9.90) | 5.41 (1.90, 17.20) | | |
| | Vessels and bronchi (not patent) | 8.89 (3.40, 27.91) | 10.00 (2.79, 44.16) | | |
| | Dots | 0.12 (0.05, 0.27) | 2.88 (0.87, 10.77) | | |
| Radiomics-added model ^b | Spiculation | 5.09 (2.43, 11.40) | 3.77 (1.28, 12.29) | 0.929 | 0.877 |
| | Satellite nodule | 0.12 (0.05, 0.27) | 0.05 (0.01, 0.16) | | |
| | Echogenicity | 4.74 (2.37, 9.90) | 5.54 (1.77, 20.29) | | |
| | Vessels and bronchi (not patent) | 8.89 (3.40, 27.91) | 4.65 (1.14, 22.05) | | |
| | Shape, polygonal | 0.03 (0.00, 0.13) | 0.06 (0.00, 0.45) | | |
| | Shape, lobulated or complex | 3.19 (1.62, 6.40) | 1.07 (0.32, 3.35) | | |
| | CRP | 0.55 (0.29, 0.83) | 0.63 (0.26, 0.96) | | |
| | Arc | 7.04 (3.24, 16.78) | 2.39 (0.70, 9.14) | | |
| | Min-HIST | 1.05 (1.01, 1.09) | 1.03 (0.99, 1.10) | | |

Note: In clinical factor model, multivariate analysis OR (95% CI) (in bold).

Abbreviations: AUC, area under curve; CI, confidence interval; CRP, C-reactive protein; CT, computed tomography; Min-HIST, minimum histogram; OR, odds ratio; US, ultrasonography.

^aClinical factor model is based on clinical demographics, CT, and US findings.

^bRadiomics-added model is based on radiomics from US images as well as demographics, clinical factors, CT, and US findings.

share the same gray level intensity. The radiomics features were automatically extracted for all given ROIs for each patient using the PyRadiomics package implemented in Python (<https://pyradiomics.readthedocs.io/en/latest/>).¹⁸

In addition to radial EBUS-derived radiomics variables, semantic variables extracted from chest CT images and ultrasound images were also included in our model. All CT image findings were analyzed for the following features: consolidation size of tumor, location (upper lobe), type (solid or partial-solid), nodule shape (round, polygonal, lobulated or complex), spiculation, bronchus sign, and presence of satellite nodules. All radial EBUS image findings were analyzed for the following features: echogenicity (homogeneous or heterogeneous), attenuation (maintenance of echogenicity supposing midline as a fiducial line), margin (regular or irregular), shape (round or complex), presence of dots or a linear arc, and patency of vessels and bronchi, along with the extracted ultrasound radiomic features.¹⁴

Statistical analysis

The χ^2 test was used to compare categorical variables, and the nonparametric Mann–Whitney U test was used to compare continuous variables between the training set and validation set and between the benign and malignant groups in the training and validation sets.

For the clinical factor model, demographic, clinical factors, CT imaging features, and radial EBUS imaging features were used as inputs. Variables with $p < 0.1$ in the univariate logistic regression were selected, and a backward selection multivariate logistic regression analysis was conducted to compare the potential predictors. For the radiomics-added model, demographic, clinical factors, CT imaging features,

and both the semantic and radiomic radial EBUS imaging features were used as inputs. Variables were selected through extreme gradient boosting, and a backward selection multivariate logistic regression was conducted to compare potential predictors. To assess the performances of the prediction models, the area under the curve (AUC) values were calculated. The overall research flow is shown in Figure 2.

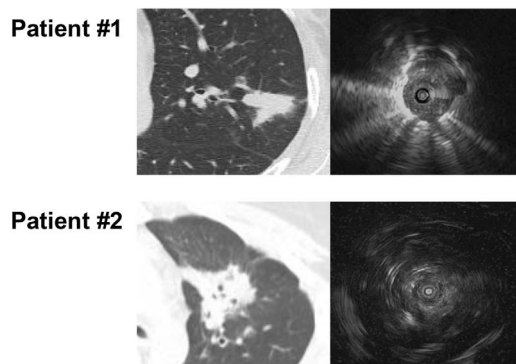
All statistical analyses were performed using R software (version 4.0.4; R Foundation for Statistical Computing). All reported p values are two-sided, and $p < 0.05$ was considered statistically significant.

RESULTS

Among the 494 patients from 2017 to 2018, 282 patients were positive for malignancy, and 212 patients were pathologically diagnosed as indeterminate (Figure 1). Forty-seven patients were lost to follow up, and eight patients were excluded because of radial EBUS image loss or poor radial EBUS image quality. Therefore, 157 patients (67 benign and 90 malignant) were analyzed for the training set. Among the 229 patients from 2019 to 2020, 213 patients were diagnosed as indeterminate and 55 patients were excluded because of a lack of follow-up information or image quality. Consequently, 158 patients (63 benign and 95 malignant) were analyzed.

Table 1 describes the demographic characteristics and CT and radial EBUS image features of the training and validation sets. The two sets did not differ significantly in final diagnosis, demographic characteristics, or chest CT findings. The factors that showed significant differences in the radial EBUS findings were tumor margin ($p = 0.001$) and patency of the vessels and bronchi ($p = 0.047$). Table 2 subdivides

a

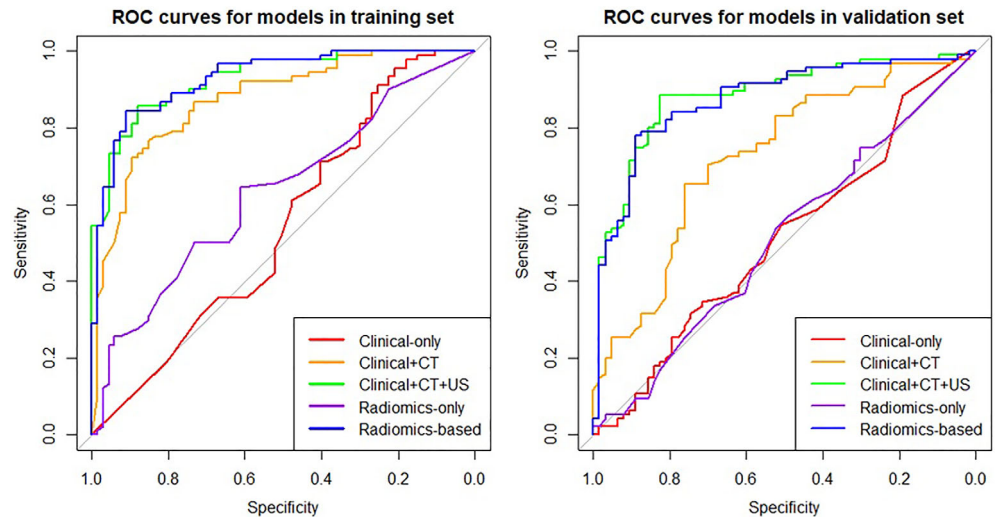


b

| | Spiculation | Shape, polygonal | Shape, lobulated/complex | Satellite nodule | CRP | Echogenicity | Linear arc | Vessels and bronchi | Min_HIST |
|------------|-------------|------------------|--------------------------|------------------|------|---------------|------------|---------------------|----------|
| Patient #1 | No | No | No | Yes | 0.16 | Homogeneous | No | Patent | 0 |
| Patient #2 | Yes | No | Yes | No | 0.04 | Heterogeneous | Yes | Not patent | 30 |

FIGURE 3 Representative lung CT images (left) and radial EBUS images (right) of two patients are shown in (a). Patient 1 was pathologically diagnosed as benign, and patient 2 was diagnosed as malignant. The variables in the radiomics-added model and individual patient data are listed in (b). Factors indicating malignancy, such as spiculation, lobulated or complex shape, absence of satellite nodules, heterogeneous echogenicity, presence of linear arc, and no patency of vessels and bronchi are observable in patient 2. A relatively low CRP value and high value of minimum histogram are also observed in patient 2, which is consistent with the results of the radiomics-added model. CT, computed tomography; radial EBUS, radial probe endobronchial ultrasound; CRP, C-reactive protein.

FIGURE 4 The ROC curves for the clinical-only model, clinical + CT model, clinical + CT + US model (clinical factor model), radiomics-only model, and radiomics-based model (radiomics-added model) in the training and validation sets. The prediction performance of the radiomics-added model and clinical + CT + US model is superior to that of the other models in the validation set, but they do not differ significantly from each other. ROC, receiver operating characteristic; CT, computed tomography; US, ultrasonography.



each set to compare the characteristics of patients with benign and malignant lesions. There was a borderline significant difference in age between the groups in the validation set ($p = 0.045$). Upper lobe, spiculation, bronchus sign, and satellite nodules in the chest CT findings differed significantly between the groups in the training set, whereas upper lobe ($p = 0.696$), spiculation ($p = 0.183$), and bronchus sign ($p = 0.275$) did not differ significantly in the validation set. The echogenicity in the radial EBUS findings differed significantly between the groups with benign and malignant lesions in both sets ($p < 0.001$).

Selected variables and model performances

Six variables were selected for the clinical factor model: three variables from the CT image findings (upper lobe, spiculation, and satellite nodules) and three from the radial EBUS findings (echogenicity, dots, and patency of the vessels and bronchi). The malignancy prediction performance for the clinical model, calculated as the AUC, was 0.910 in the training set and 0.891 in the validation set (Table 3).

For the radiomics-added model, nine variables were selected: four from the CT image findings (satellite nodule, spiculation, polygonal shape, and lobulated or complex shape), three from the radial EBUS findings (patency of vessels and bronchi, echogenicity, and linear arc), one from the peripheral blood lab data (CRP), and one radiomics feature from the radial EBUS image (minimum histogram). Examples of CT and ultrasound images from patients with benign and malignant lesions and their individual features in the radiomics-added model are shown in Figure 3. The performance of the radiomics-added model was 0.929 in the training set and 0.877 in the validation set. The malignancy prediction performance of the radiomics-added model was therefore, slightly higher than that of the clinical factor model in the training set and comparable to that of the clinical factor model in the validation set ($p = 0.45$). The receiver operating characteristic (ROC) curves for these models are shown in Figure 4.

DISCUSSION

The diagnosis of peripheral pulmonary lesions remains a challenge in clinical practice. The main challenges include approaching the targeted lesions and recognizing where to take biopsies. Technological advances such as radial EBUS help clinicians by providing real-time procedural feedback about target lesion locations.¹⁹ However, because the tissue samples are necessarily small, the results of radial EBUS are not always enough to make a final diagnosis, which complicates subsequent patient management. In a meta-analysis conducted in 2017, the overall diagnostic yield for radial EBUS was reported to be 70.6%.²⁰ However, in real-world data, the diagnostic yield has been suggested to be even lower, ~57%.²¹ Indeed, when we included only cases pathologically confirmed for final diagnosis using radial EBUS alone, our cohort showed a diagnostic yield of 57% as well.

To diagnose the indeterminate cases, several attempts have been made to extract additional information from radial EBUS images. Zheng et al.²² built a predictive model with semantic features from radial EBUS images (size, shape, echogenicity, margin, blood vessel, and linear-discrete air bronchogram), and achieved an accuracy of 82.76%. Bradiei et al.²³ analyzed radial EBUS images using customized software and computed grayscale statistics (maximum, mean, standard deviation, and entropy) to predict malignancy and achieved accuracy up to 85%. Our radiomics-added model uses demographics, clinical factors, chest CT image findings, and semantic and radiomic features from radial EBUS images and achieved a performance of 92.9% in the training set and 87.7% in the validation set.

In this study, we selected nine variables for our radiomics-added model. The four variables from the chest CT findings are known to be associated with malignancy. Satellite nodules are usually defined as small discrete shadows located near the main lesion²⁴ and are frequently seen in benign nodules in tuberculosis-endemic areas.²⁵ Spiculation is associated with the radial extension of malignant cells and is known to have a

high predictive value for malignancy.²⁶ A lobulated or complex tumor shape is more likely to be associated with malignancy than a round or polygonal shape.²⁷

Three variables were derived from the radial EBUS image findings. Echogenicity on radial EBUS images is closely related to the arrangement of cells and quantity of fibrous stroma.²⁸ Therefore, the loss of normal tissue and irregular tumor growth with central fibrosis and necrosis causes heterogeneous features to appear on EBUS images.⁶ The patency of the vessels and bronchi on radial EBUS images is understood to reflect the degree of anatomic structure preservation in the lung parenchyma because that structure usually becomes distorted as tumor volume increases.²⁹ A linear arc denotes irregular hyper-echoic patterns within lesions in radial EBUS images, and it corresponds to residual air in the alveoli, which is indicative of well-differentiated adenocarcinoma.⁶ Among the demographic and peripheral blood lab data, CRP showed statistical significance and was included. CRP is a classical acute-phase protein indicating inflammation, but it is also moderately elevated during chronic inflammatory disease and cancer.³⁰

In addition, we hypothesized that adding radiomics variables would improve our prediction model. Radiomics can be applied to various conditions, but it is most promising in the field of oncology. Whereas current radiological practice is generally qualitative and measures tumor size only via a one-dimensional or two-dimensional axis diameter, tumor characterization based on radiomics can reflect the complexity of tumor morphology or tumor texture, which implicate tumor behavior and changes.³¹ Multiple studies using radiomics have shown that it can improve the characterization of tumor biology phenotypes, prediction of tumor prognosis, and assessment of the tumor treatment response.^{32–35}

We reviewed the radiomics features available in radial EBUS and chose minimum histogram, a radiomic feature that shows the lowest echogenic tumor pixel intensity within the defined lesion ROI^{36,37} and can therefore, reflect microscopic necrosis or a less-viable area within the tumor that cannot be seen by the naked eye. Tumor necrosis usually manifests as coagulative necrosis caused by chronic ischemia or hypoxia.^{38,39} Moreover, the most common types of benign pulmonary necrotic lesions are lung abscesses and tuberculosis, and they are usually caused by an inflammatory response to a microbial infection.⁴⁰ Necrotic tissues from lung abscesses mainly contain highly viscous pus,⁴⁰ and tuberculosis exhibits caseous necrosis with rich lipid content.³⁸ Therefore, their different biological traits could be reflected in pixel distribution of ultrasound images and discriminated sensitively by our radiomic variable.⁴¹

In the past, one of the main challenges of radiomics was the manual delineation of each datapoint, which is time consuming and prone to high inter-observer variability.⁴² However, many powerful open-source and commercial platforms have recently become available to process and extract features from medical images, making radiomics-based analyses easier and more accessible.⁴³ Our radiomics-based approach could improve prediction performance without much effort, which gives our study high practical usability in clinical settings.

Nonetheless, our study has several limitations. First, it was a single-center retrospective study with a small number of patients, which could limit its generalizability. However, to maintain the independence of the test sets, we constructed two separate cohorts recruited in different time periods to validate our model. Second, we selected minimum histogram as a radiomic variable for our radiomics-added model based on its clinical implications and statistical significance in the univariate analysis ($p < 0.01$), but our radiomics-added model is only superior to the clinical factor model in training set; it does not show superiority in validation set. Radial EBUS itself is a procedure that is highly dependent on operator factors, and the quality of the captured images can have high inter-observer variability. To obtain quality radial EBUS image, it requires the skills of the clinicians to precisely detect the lesion of the interest and reproduce the same radial EBUS image. In addition, radial EBUS image may not fully convey the characteristics of the lesion. For instance, if lesions coexist with atelectatic proportion, radiologic features from radial EBUS may have been distorted. This might have lowered the prediction performance of our radiomics variable. Further studies with a bigger sample size are needed.

In conclusion, we demonstrated a radiomics-added, malignancy prediction model that can categorize lesions with non-diagnostic lung biopsy results. With ongoing studies and appropriate validation, this model could potentially facilitate decision-making for subsequent clinical management.

AUTHOR CONTRIBUTIONS

All authors had full access to the data in the study and take responsibility for the integrity of the data and the accuracy of the data analysis. Conceptualization: H.Y.L. and K.J.L., Formal analysis: J.H.C. and J.H.A., Investigation: S.M.J. and M.K.K., Software: J.H.K. and Y.J.O., Visualization: J.H.C., S.M.Z., and J.H.K., Writing – Original draft: J.H.C. and S.M.Z., Writing – Review & Editing: H.Y.L. and K.J.L.

ACKNOWLEDGMENT

This work was supported by the Future Medicine 20*30 Project of the Samsung Medical Center (SMO1220071) and by a National Research Foundation of Korea (NRF) grant funded by the Korean government (MSIT) (NRF-2022R1A2C1003999).

ORCID

You Jin Oh  <https://orcid.org/0000-0002-2801-4100>

Ho Yun Lee  <https://orcid.org/0000-0001-9960-5648>

REFERENCES

1. Herth FJ, Ernst A, Becker HD. Endobronchial ultrasound-guided transbronchial lung biopsy in solitary pulmonary nodules and peripheral lesions. *Eur Respir J*. 2002;20(4):972–4.
2. Paone G, Nicastrì E, Lucantoni G, dello Iacono R, Battistoni P, D'Angeli AL, et al. Endobronchial ultrasound-driven biopsy in the diagnosis of peripheral lung lesions. *Chest*. 2005;128(5):3551–7.
3. She Y, Zhao L, Dai C, Ren Y, Jiang G, Xie H, et al. Development and validation of a nomogram to estimate the pretest probability of cancer in Chinese patients with solid solitary pulmonary nodules: a multi-institutional study. *J Surg Oncol*. 2017;116(6):756–62.

4. Swensen SJ et al. The probability of malignancy in solitary pulmonary nodules. Application to small radiologically indeterminate nodules. *Arch Intern Med.* 1997;157(8):849–55.
5. Nguyen P, Bashirzadeh F, Hundloe J, Salvado O, Dowson N, Ware R, et al. Grey scale texture analysis of endobronchial ultrasound mini probe images for prediction of benign or malignant aetiology. *Respirology.* 2015;20(6):960–6.
6. Kurimoto N, Murayama M, Yoshioka S, Nishisaka T. Analysis of the internal structure of peripheral pulmonary lesions using endobronchial ultrasonography. *Chest.* 2002;122(6):1887–94.
7. Song J, Yin Y, Wang H, Chang Z, Liu Z, Cui L. A review of original articles published in the emerging field of radiomics. *Eur J Radiol.* 2020;127:108991.
8. Aerts HJ. The potential of radiomic-based phenotyping in precision medicine: a review. *JAMA Oncol.* 2016;2(12):1636–42.
9. Mayerhoefer ME, Materka A, Langs G, Häggström I, Szczypiński P, Gibbs P, et al. Introduction to Radiomics. *J Nucl Med.* 2020;61(4):488–95.
10. Thawani R, McLane M, Beig N, Ghose S, Prasanna P, Velcheti V, et al. Radiomics and radiogenomics in lung cancer: a review for the clinician. *Lung Cancer.* 2018;115:34–41.
11. Xu X, Zhang HL, Liu QP, Sun SW, Zhang J, Zhu FP, et al. Radiomic analysis of contrast-enhanced CT predicts microvascular invasion and outcome in hepatocellular carcinoma. *J Hepatol.* 2019;70(6):1133–44.
12. Yoon HJ, Park H, Lee HY, Sohn I, Ahn J, Lee SH. Prediction of tumor doubling time of lung adenocarcinoma using radiomic margin characteristics. *Thorac Cancer.* 2020;11(9):2600–9.
13. Wu G, Woodruff HC, Shen J, Refaee T, Sanduleanu S, Ibrahim A, et al. Diagnosis of invasive lung adenocarcinoma based on chest CT Radiomic features of part-solid pulmonary nodules: a multicenter study. *Radiology.* 2020;297(2):451–8.
14. Zo S, Woo SY, Kim S, Lee JE, Jeong BH, Um SW, et al. Predicting the risk of malignancy of lung nodules diagnosed as indeterminate on radial endobronchial ultrasound-guided biopsy. *J Clin Med.* 2020;9(11):3652–62.
15. Cho HH, Lee G, Lee HY, Park H. Marginal radiomics features as imaging biomarkers for pathological invasion in lung adenocarcinoma. *Eur Radiol.* 2020;30(5):2984–94.
16. Moon SM, Choe J, Jeong BH, Um SW, Kim H, Kwon OJ, et al. Diagnostic performance of radial probe endobronchial ultrasound without a guide-sheath and the feasibility of molecular analysis. *Tuberc Respir Dis.* 2019;82(4):319–27.
17. Choe J, Lee SM, do KH, Lee G, Lee JG, Lee SM, et al. Deep learning-based image conversion of CT reconstruction kernels improves Radiomics reproducibility for pulmonary nodules or masses. *Radiology.* 2019;292(2):365–73.
18. van Griethuysen JJM, Fedorov A, Parmar C, Hosny A, Aucoin N, Narayan V, et al. Computational Radiomics system to decode the radiographic phenotype. *Cancer Res.* 2017;77(21):e104–7.
19. Chen A, Chenna P, Loissele A, Massoni J, Mayse M, Misselhorn D. Radial probe endobronchial ultrasound for peripheral pulmonary lesions. A 5-year institutional experience. *Ann Am Thorac Soc.* 2014; 11(4):578–82.
20. Ali MS, Trick W, Mba BI, Mohanany D, Sethi J, Musani AI. Radial endobronchial ultrasound for the diagnosis of peripheral pulmonary lesions: a systematic review and meta-analysis. *Respirology.* 2017; 22(3):443–53.
21. Ost DE, Ernst A, Lei X, Kovitz KL, Benzaquen S, Diaz-Mendoza J, et al. Diagnostic yield and complications of bronchoscopy for peripheral lung lesions. Results of the AQuIRE registry. *Am J Respir Crit Care Med.* 2016;193(1):68–77.
22. Zheng X, Wang L, Chen J, Xie F, Jiang Y, Sun J. Diagnostic value of radial endobronchial ultrasonographic features in predominant solid peripheral pulmonary lesions. *J Thorac Dis.* 2020;12(12):7656–65.
23. Badiei A, Nguyen P, Jersmann H, Wong M. Radial endobronchial ultrasound greyscale texture analysis using whole-lesion analysis can characterise benign and malignant lesions without region-of-interest selection bias. *Respiration.* 2019;97(1):78–83.
24. Iversen M. Synopsis of diseases of the chest (2nd edn). *Respir Med.* 1995;89:643–4.
25. Kim H et al. Predictors for benign solitary pulmonary nodule in tuberculosis-endemic area. *Korean J Intern Med.* 2001;16(4):236–41.
26. Winer-Muram HT. The solitary pulmonary nodule. *Radiology.* 2006; 239(1):34–49.
27. Xu DM, van Klaveren RJ, de Bock GH, Leusveld A, Zhao Y, Wang Y, et al. Limited value of shape, margin and CT density in the discrimination between benign and malignant screen detected solid pulmonary nodules of the NELSON trial. *Eur J Radiol.* 2008;68(2):347–52.
28. Kuo CH, Lin SM, Chen HC, Chou CL, Yu CT, Kuo HP. Diagnosis of peripheral lung cancer with three echoic features via endobronchial ultrasound. *Chest.* 2007;132(3):922–9.
29. Wang JC, Sone S, Feng L, Yang ZG, Takashima S, Maruyama Y, et al. Rapidly growing small peripheral lung cancers detected by screening CT: correlation between radiological appearance and pathological features. *Br J Radiol.* 2000;73(873):930–7.
30. Allin KH, Nordestgaard BG. Elevated C-reactive protein in the diagnosis, prognosis, and cause of cancer. *Crit Rev Clin Lab Sci.* 2011; 48(4):155–70.
31. Kumar V, Gu Y, Basu S, Berglund A, Eschrich SA, Schabath MB, et al. Radiomics: the process and the challenges. *Magn Reson Imaging.* 2012;30(9):1234–48.
32. Son JY, Lee HY, Kim JH, Han J, Jeong JY, Lee KS, et al. Quantitative CT analysis of pulmonary ground-glass opacity nodules for distinguishing invasive adenocarcinoma from non-invasive or minimally invasive adenocarcinoma: the added value of using iodine mapping. *Eur Radiol.* 2016;26(1):43–54.
33. Lee G, Bak SH, Lee HY. CT radiomics in thoracic oncology: technique and clinical applications. *Nucl Med Mol Imaging.* 2018;52(2):91–8.
34. Sun Y, Li C, Jin L, Gao P, Zhao W, Ma W, et al. Radiomics for lung adenocarcinoma manifesting as pure ground-glass nodules: invasive prediction. *Eur Radiol.* 2020;30(7):3650–9.
35. Mu W, Jiang L, Zhang JY, Shi Y, Gray JE, Tunali I, et al. Non-invasive decision support for NSCLC treatment using PET/CT radiomics. *Nat Commun.* 2020;11(1):5228.
36. Eloyan A, Yue MS, Khachatryan D. Tumor heterogeneity estimation for radiomics in cancer. *Stat Med.* 2020;39(30):4704–23.
37. Just N. Improving tumour heterogeneity MRI assessment with histograms. *Br J Cancer.* 2014;111(12):2205–13.
38. Adigun R, Basit H, Murray J. Cell liquefactive necrosis. *StatPearls Treasure Island (FL): StatPearls Publishing LLC; 2022, StatPearls Publishing Copyright © 2022.*
39. Li Q, Fan X, Luo TY, Lv FJ, Huang XT. Differentiating malignant and benign necrotic lung lesions using kVp-switching dual-energy spectral computed tomography. *BMC Med Imaging.* 2021;21(1):81.
40. Kuhajda I et al. Lung abscess-etiology, diagnostic and treatment options. *Ann Transl Med.* 2015;3(13):183.
41. Nadal Desbarats L, Herlidou S, de Marco G, Gondry-Jouet C, le Gars D, Deramond H, et al. Differential MRI diagnosis between brain abscesses and necrotic or cystic brain tumors using the apparent diffusion coefficient and normalized diffusion-weighted images. *Magn Reson Imaging.* 2003;21(6):645–50.
42. Parmar C, Rios Velazquez E, Leijenaar R, Jermoumi M, Carvalho S, Mak RH, et al. Robust Radiomics feature quantification using semiautomatic volumetric segmentation. *PLoS One.* 2014;9(7):e102107.
43. Avanzo M et al. Machine and deep learning methods for radiomics. *Med Phys.* 2020;47(5):e185–202.

How to cite this article: Choi J, Zo S, Kim JH, Oh YJ, Ahn JH, Kim M, et al. Nondiagnostic, radial-probe endobronchial ultrasound-guided biopsy for peripheral lung lesions: The added value of radiomics from ultrasound imaging for predicting malignancy. *Thorac Cancer.* 2023;14(2):177–85. <https://doi.org/10.1111/1759-7714.14730>